Temporal stimulated intersubband emission of photoexcited electrons

F. T. Vasko*

Institute of Semiconductor Physics, NAS Ukraine, Pr. Nauki 41, Kiev, 03028, Ukraine

A. Hernández-Cabrera[†] and P. Aceituno

Dpto. Física Básica, Universidad de La Laguna, La Laguna, 38206-Tenerife, Spain

We have studied the transient evolution of electrons distributed over two levels in a wide quantum well, with the two levels below the optical phonon energy, after an ultrafast interband excitation and cascade emission of optical phonons. If electrons are distributed near the top of the passive region, a temporal negative absorption appears to be dominant in the intersubband response. This is due to the effective broadening of the upper level state under the optical phonon emission. We have then considered the amplification of the ground mode in a THz waveguide with a multiquantum well placed at the center of the cavity. A huge increase of the probe signal is obtained, which permits the temporal stimulated emission regime of the photoexcited electrons in the THz spectral region.

I. INTRODUCTION

The temporal emission of THz radiation due to the coherent oscillations of electrons under ultrafast interband excitation have been studied during last decades (see Ref. 1 for a review). The duration of the generated THz pulse is in the order of picoseconds due to effective relaxation of the coherent response. Furthermore, the steady-state spontaneous and stimulated emissions from different semiconductor structures under an electric field pump have been demonstrated (see Ref. 2, and references therein). However, the character of the temporal evolution of photoexcited electrons during the noncoherent stage of the relaxation is not completely understood yet. After the initial photoexcitation and emission of the optical phonon cascade, which takes place in a picosecond time interval, which have been considered in detail (see Refs. 1 and 3–5, and references therein), a nonequilibrium distribution appears in the passive region, with the energy ε_{ex} less than the optical phonon energy $\hbar\omega_o$.[6] A temporal evolution of this distribution takes place during a nanosecond time interval. This evolution is caused by the quasielastic scattering of electrons with acoustic phonons. Due to the partial inversion of this distribution, a set of peculiarities of the magnetotransport coefficients, such as *the total negative conductivity*, or the negative cyclotron absorption, appears.[7]

For the wide quantum well (QW) case under consideration, with two levels in the passive region, the character of the evolution appears to be more complicated due to the interlevel scattering. The regime of *negative absorption* is possible due to a more effective broadening of the absorption [dashed arrow in Fig. 1(a)] in comparison with the intersubband emission (solid arrow). Such regime appears because the absorption process involves the state in the active region for which the optical phonon emission is allowed. Thus, a question arises about the temporal stimulated emission coming from a wide multiple quantum well (MQW) structure placed at the center of THz waveguide, as it is shown in Fig. 1(b). In this paper we consider the amplification of the probe ground mode in the THz resonator caused by the temporal

negative absorption described above. We have found a huge amplification of the probe signal, so that it may be concluded that a temporal stimulated emission takes place in the THz waveguide with weak cavity losses and with the MQW structure placed at the center.

Our study is based on the general kinetic equation for the distribution function in the conduction c band $f_{\alpha t}$, written in the following form:

$$\frac{\partial f_{\alpha t}}{\partial t} = G_{\alpha t} + J(f|\alpha t), \qquad (1)$$

where $G_{\alpha t}$ and $J(f|\alpha t)$ are the photogeneration rate and collision integral for the c-band state α, respectively. The generation rate in Eq. (1) is given by[4]
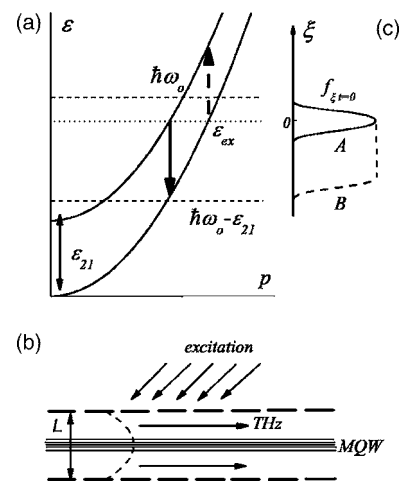

FIG. 1. Scheme of the intersubband transitions for electrons with energies near the top of the passive region (the stimulated emission and absorption are shown by the solid and dashed arrows, respectively) (a), the geometry of the THz waveguide with the MQW structure in the center (b), and the initial distributions over the passive region for the cases A and B (c).

$$G_{\alpha t} = w_t^2 \sum_l g_l \delta_{\Delta_l}(\varepsilon_\alpha - \varepsilon_l), \qquad (2)$$

where w_t is the form factor of the excitation field with the pulse duration τ_p, the factor g_l describes the relative contributions of different valence v-band states (heavy and light holes confined in the wide QW). The shape of the photoexcited distribution is given by the Gaussian function $\delta_\Delta(E) = \exp[-(E/\Delta)^2]/(\sqrt{\pi}\Delta)$ with the width Δ and centered at $E = 0$. The width of these functions is determined by two different broadening processes: the spreading due to the energy-time uncertainty relation and the anisotropy of the valence band. These values are estimated by the energy values $\hbar/\tau_p$ and $\beta\varepsilon_l$, respectively, where $\beta \ll 1$ is the anisotropy parameter. Under the optical phonon emission an additional broadening appears. Such a broadening is caused by the weak phonon dispersion, and characterized by the energy $\delta\varepsilon_{opt}$.

Thus, the initial conditions in the passive region, after the picosecond stage of the evolution due to optical phonon emission, are obtained from Eqs. (1) and (2) in the following manner:

$$f_{j\varepsilon t=0} = \sum_l \frac{n_l^{(j)}}{\rho_{2D}} \delta_{\Delta_l^{(j)}}(\varepsilon - \varepsilon_l^{(j)}). \qquad (3)$$

Here ρ_{2D} is the 2D density of states, the total broadening energy is determined as $\Delta_l^{(j)} \sim \max(\hbar/\tau_p, \beta\varepsilon_l, \delta\varepsilon_{opt})$, and $j = 1, 2$ are the corresponding two levels in the passive region. Below, we will concentrate solely on two models of the initial distribution: a narrow Gaussian peak (case A) and a flat distribution over the interval $(\hbar\omega_o - \varepsilon_{21}, \hbar\omega_o)$ (case B), which are shifted from the boundary of the passive region, as Fig. 1(c) shows. Both distributions are relaxed between the subbands and to the bottom of the passive region. The temporal intersubband response is determined by the interlevel redistribution of the population.

The analysis we will carry out next is divided in two sections. The temporal evolution of the distribution over the two subbands is described in Sec. II, including the consideration of the resonant intersubband response. The results for the transient amplification of a probe mode in the THz waveguide are given in Sec. III, with our conclusions presented in Sec. IV. The Appendix contains the microscopical evaluation of the broadening energy for the intersubband transitions.

II. TEMPORAL EVOLUTION OF THE ELECTRONIC DISTRIBUTION

We shall now turn to consider the temporal evolution of the photoexcited electrons in the passive region caused by the quasielastic scattering with acoustic phonons. Since the above-discussed initial distributions are isotropic over the 2D plane, one has to consider the energy-dependent distribution functions $f_{1,2\varepsilon t}$ governed by the system of kinetic equations

$$\frac{\partial f_{1\varepsilon t}}{\partial t} = J(f|1\varepsilon t) - \nu_{\varepsilon - \varepsilon_{21}}(f_{1\varepsilon t} - f_{2\varepsilon - \varepsilon_{21}t}),$$
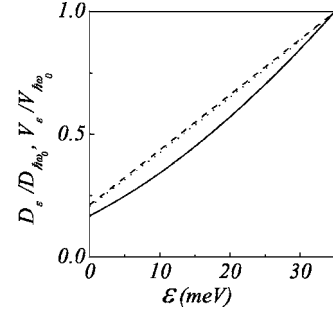

FIG. 2. Normalized diffusion and drift coefficients vs energy. Solid and dotted curves: diffusion coefficient for $T = 4.2$ K and $T = 20$ K, respectively. Dashed line: drift coefficient which is independent of T.

$$\frac{\partial f_{2\varepsilon t}}{\partial t} = J(f|2\varepsilon t) + \nu_{\varepsilon + \varepsilon_{21}}(f_{1\varepsilon + \varepsilon_{21}t} - f_{2\varepsilon t}). \qquad (4)$$

Moreover, these equations are written for the intervals $(0, \hbar\omega_o)$ and $(\varepsilon_{21} - \hbar\omega_o, \hbar\omega_o)$ for the first and second subbands, respectively. The interlevel relaxation frequency is introduced here as

$$\nu_\varepsilon = \theta(\varepsilon) \frac{2\pi}{\hbar} \int_0^{2\pi} \frac{d\varphi}{2\pi} \sum_{\mathbf{p}', q_\perp} |C_Q|^2$$
$$\times |\langle 2|e^{-iq_\perp z}|1\rangle|^2 (2N_Q + 1)\delta(\varepsilon - \varepsilon'), \qquad (5)$$

where C_Q is the matrix element for the bulk electron-phonon interaction with the acoustic phonons. The quasielastic collision integral in the jth subband is reached as

$$J(f|j\varepsilon t) = \frac{\partial}{\partial\varepsilon}\left(D_{j\varepsilon}\frac{\partial f_{j\varepsilon t}}{\partial\varepsilon} + V_{j\varepsilon}f_{j\varepsilon t}\right). \qquad (6)$$

The diffusion and drift coefficients in Eq. (6), $D_{j\varepsilon}$ and $V_{j\varepsilon}$, are determined as follows:

$$\begin{vmatrix} D_{j\varepsilon} \\ V_{j\varepsilon} \end{vmatrix} = \frac{\pi\rho_{2D}}{\hbar} \int_0^{2\pi} \frac{d\varphi}{2\pi} \int_{-\infty}^\infty \frac{dq_\perp}{2\pi} V|C_Q|^2$$
$$\times |\langle j|e^{-iq_\perp z}|j\rangle|^2 \begin{vmatrix} (2N_Q + 1)(\hbar\omega_Q)^2/2 \\ \hbar\omega_Q \end{vmatrix}, \qquad (7)$$

where $N_Q = [\exp(\hbar\omega_Q/T) - 1]^{-1}$. A similar description of the quasi-elastic relaxation in a two-level system was discussed in Ref. 8.

Since the elastic interlevel relaxation is the dominant process for the energy interval $(\varepsilon_{21}, \hbar\omega_o)$, one obtains $f_{1\varepsilon t} \approx f_{2\varepsilon - \varepsilon_{21}t} \simeq f_{\varepsilon t}$ if t exceeds the interlevel relaxation time. Using the energy variable $\xi = \varepsilon - \hbar\omega_o$ we determine the distribution function $f_{\xi + \hbar\omega_o t} \equiv f_{\xi t}$ from the diffusion-drift equation for the two-level zone of the passive region, $0 > \xi > \varepsilon_{21} - \hbar\omega_o$:

$$\frac{\partial f_{\xi t}}{\partial t} = \frac{\partial}{\partial\xi}\left(D_\xi \frac{\partial f_{\xi t}}{\partial\xi} + V_\xi f_{\xi t}\right), \qquad (8)$$

where D_ξ and V_ξ are the energy diffusion and the drift coefficients determined by Eq. (7). These coefficients are shown in Fig. 2 for a GaAs-based QW which is 320 Å wide, with an
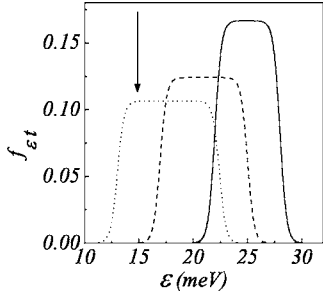
FIG. 3. Evolution of the electron distribution for case B. Solid, dashed, and dotted curves correspond to $t=0$, 1.6, and 3.2 ns, respectively. Vertical arrow indicates the position of ε_{21}.

interlevel distance $\varepsilon_{21}=15$ meV and for two different temperatures $T=4.2$ K and $T=20$ K. Thus, the normalization coefficients $D_{\hbar\omega_o} \equiv D_{\xi=0} = 3.91 \times 10^9$ meV^2/s and 9.55×10^9 meV^2/s for $T=4.2$ K and $T=20$ K, respectively. Another coefficient, which is independent on the temperature, is $V_{\hbar\omega_o} \equiv V_{\xi=0} = 5.22 \times 10^9$ meV/s. Note that $D/V \simeq T$ for $T = 20$ K while a visible distinction of energy dependencies appears at $T=4$ K. We use below the energy-independent coefficients $V=3.5 \times 10^9$ meV/s, and $D=2.2 \times 10^9$ meV^2/s and 6.2×10^9 meV^2/s for $T=4.2$ K and $T=20$ K, respectively. This approximation is valid within an accuracy better than 20% for the numerical parameters in the interval ($\hbar\omega_o - \varepsilon_{21}, \hbar\omega_o$) considered below. Another important parameter is the interlevel relaxation time, ν_ε^{-1}, which was assumed to be shorter than the time scales of Figs. 3 and 4. Actually, for the above used parameters, ν_ε^{-1} varies from 0.21 to 0.19 ns over the passive region.

Equation (8) may be considered with the zero boundary conditions at $\xi \rightarrow \pm\infty$ if $\hbar\omega_o - \varepsilon_{21} > \varepsilon_{21}$. The initial distribution is located in the region $\xi < 0$, and electrons do not reach the bottom of the second level, i.e., $\xi > -\varepsilon_{21}$. For the case A we use the initial condition, $f_{\xi t=0} = n_{ex}\delta_\Delta(\xi-\xi_{ex})/2\rho_{2D}$, where n_{ex} is the total excited concentration, $\xi_{ex} \simeq -9$ meV is the excitation energy, and the half-width of the peak is equal to 2.5 meV. Thus, the solution for Eq. (8) may be written as the moving peak

$$f_{\xi t} = \frac{n_{ex}}{2\rho_{2D}} \delta_{\Delta_t}(\xi + Vt - \xi_{ex}) \qquad (9)$$

with the time-dependent half-width $\Delta_t = \sqrt{\Delta^2 + 4Dt}$. For the case B, the broadening of the stepped distribution is equal to
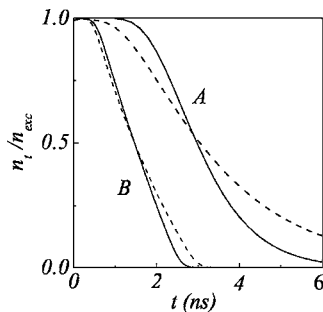

FIG. 4. Temporal evolution of the concentration for the distributions A and B, at $T=4.2$ K and 20 K (solid and dashed curves, respectively).

2.5 meV. The solution is given by the integral of the initial distribution multiplied by a similar to (2) form-factor. This solution is plotted in Fig. 3 for different times.

In order to describe the temporal negative absorption, we need the concentration over the negative absorption region $(\hbar\omega_o - \varepsilon_{21}, \hbar\omega_o)$ defined as $n_t = 2\rho_{2D}\int_{-\varepsilon_{21}}^{0} d\xi f_{\xi t}$. The temporal evolution of n_t, obtained with the solutions of Eq. (8) for the cases A and B, and the QW parameters detailed above, is shown in Fig. 4.

The temporal evolution of the resonant absorption of the nonequilibrium electrons is described by the real part of the conductivity (see Ref. 8 and the Appendix):

$$\text{Re } \sigma_{\delta\varepsilon,t} = \frac{e^2 |v_\perp|^2}{\varepsilon_{21}/\hbar} \frac{n_t}{2} \left(\frac{\Gamma}{\delta\varepsilon^2 + \Gamma^2} - \frac{\gamma}{\delta\varepsilon^2 + \gamma^2} \right). \qquad (10)$$

Here $\delta\varepsilon = \hbar\omega - \varepsilon_{21}$ is the detuning energy, $v_\perp$ is the intersubband velocity matrix element, Γ and γ are the broadening energy values due to the optical phonon emission and the elastic scattering, which correspond to the absorption and stimulated emission processes. Using Eq. (A11) and the parameters given above we make an estimate of $\Gamma \sim 1.3 (1.5)$meV [for $\xi_{ex} = -4(-9)$ meV, respectively], so that $\Gamma \gg \gamma$ and one obtains Re $\sigma_{\delta\varepsilon=0,t} < 0$. The contribution to Re $\sigma_{\delta\varepsilon,t}$ from electrons distributed over the region $-\varepsilon_{21} > \xi > \varepsilon_{21} - \hbar\omega_o$ is equal to zero due to the same broadening of the absorption and emission processes. We have also supposed that electrons are absent from the region $\xi < \varepsilon_{21} - \hbar\omega_o$, where only the absorption due to transitions $1 \rightarrow 2$ is possible.

III. TRANSIENT AMPLIFICATION

We then consider the amplification of a probe THz mode in the ideal waveguide of width L due to the temporal negative absorption discussed above. The transverse electric field in the resonator $E_{zt}^\perp \exp(-i\omega t + ikx)$ is ruled by the wave equation:

$$\left(\frac{\partial^2}{\partial z^2} - \kappa^2 \right) E_{zt}^\perp + i\epsilon \frac{2\omega}{c^2} \frac{\partial E_{zt}^\perp}{\partial t} = 0 \qquad (11)$$

with $\kappa^2 = k^2 - \epsilon\omega^2/c^2$, where ϵ is the dielectric permittivity supposed to be uniform across the structure. The boundary conditions at $z=\pm L/2$ takes the form $E_{z=\pm L/2,t}^\perp = 0$. At the center of the resonator ($z=0$), where the MQW is placed, one has to use

$$E_{zt}^\perp|_{-0}^0 = 0, \qquad \frac{\partial E_{zt}^\perp}{\partial z}\bigg|_{-0}^0 \simeq -iN\frac{4\pi\omega}{c^2}\sigma_{\delta\varepsilon,t}E_{z=0t}^\perp, \qquad (12)$$

where N is the number of wells in the structure. The initial condition for the ground mode propagating along the resonator is $E_{zt=0}^\perp = E\cos(\pi z/L)$.

Taking into account the slowness of the temporal evolution under the condition $\alpha = N\pi e^2 |v_\perp|^2 Ln_{ex}/\gamma c^2 \ll 1$ and restricting ourselves to the resonant case, $\delta\varepsilon=0$, we obtain the solution of Eqs. (11) and (12) as $E_{zt}^\perp = \mathcal{E}_t\cos(\pi z/L)$ where the time-dependent field is governed by
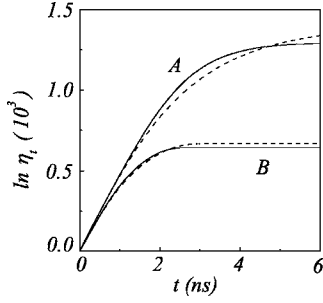
FIG. 5. Transient amplification η_t for the same conditions as in Fig. 4.

$$\frac{\partial \mathcal{E}_t}{\partial t} = \frac{n_t}{\tau^* n_{\text{ex}}} \mathcal{E}_t, \quad \frac{1}{\tau^*} = \frac{4\alpha c^2}{\epsilon \omega_{21} L^2}, \tag{13}$$

with the initial condition $\mathcal{E}_{t=0} = E$.

After averaging over the resonator, the Poynting vector along the *OX* direction is introduced as

$$S_t = \frac{kc^2}{2\pi\omega} \int dz |\mathcal{E}_{zt}|^2 \tag{14}$$

and the temporal amplification is determined as the ratio of Eq. (14) to the Poynting vector at $t=0$:

$$\eta_t = \frac{S_t}{S_{t=0}} = \exp\left(2 \int_0^t \frac{dt'}{\tau^*} \frac{n_{t'}}{n_{\text{ex}}} \right). \tag{15}$$

In Fig. 5 we plotted the logarithm of the amplification coefficient versus time for a five-layer MQW with $\gamma = 0.2$ meV under the photoexcited concentration $n_{\text{ex}} = 10^{10}$ cm^{-2}. We have also used $\epsilon = 12.9$ and $L = 19$ μm, corresponding to the ground mode propagation along the THz waveguide. One can see the saturation of $\ln \eta_t$ when n_t/n_{ex} approaches zero (see Fig. 4). The maximal value of $\ln \eta_t$ is around 10^3, i.e., a huge temporal amplification of the probe signal has been obtained. Thus, the stimulated regime of the emission should be realized in the THz waveguide with a weak damping (such waveguides have been studied recently, see Ref. 9, and references therein).

IV. CONCLUSIONS

In summary, we have considered a new noncoherent transient mechanism of the stimulated emission in the THz spectral region. The mechanism requires neither coherent response nor inverted distribution but it rather appears due to the different broadening of emission and absorption contributions in Eq. (10).

The consideration performed here is based on several assumptions. Rather than using a microscopic calculation of the photogeneration, we have used two models for initial conditions (*A* and *B*) to obtain the temporal evolution of the distribution. We have also neglected the energy dependencies of D_ξ and V_ξ in Eq. (8). In Eq. (10), which describes the intersubband response, we have neglected the Coulomb renormalization effect and taken into account that $\Gamma \gg \gamma$ as it is demonstrated in the Appendix. What is even more impor-

tant is that we have considered the low-concentration case, neglecting the electron-electron and the electron-hole scattering as well as the exciton formation processes. According to Refs. 10 and 11, these processes are not effective for the region $n_{\text{ex}} \lesssim 10^{10}$ cm^{-2}; note that $\ln \eta_t \propto n_{\text{ex}}$, so that $\ln \eta_\infty$ should be about 100 at $n_{\text{ex}} \sim 10^9$ cm^{-2}. An interesting question is the evaluation of the limiting concentration, which needs to estimate the maximal amplification, and it lies beyond the scope of this paper. We also neglected nonparabolicity of the electron dispersion law and the effect of the spatial confinement on phonons and electron-phonon interaction.[12] These approximations are generally accepted for the GaAs/AlGaAs heterostructures with the parameters used here. In addition, instead of a stimulated emission effect due to the transient negative absorption, we have calculated the amplification of a probe signal, and the role of the waveguide losses is not considered here.

To conclude, we have found a huge amplification due to the temporal negative absorption under intersubband transitions of photoexcited electrons in a wide MQW structure placed at the center of a THz resonator. We expect that the presented analysis motivates an experimental treatment of the transient stimulated emission both for the system considered and for another heterostructure with closely-spaced levels (stepped QW, tunnel-coupled structures, etc.).

APPENDIX: BROADENING OF INTERSUBBAND TRANSITIONS

Below we present the evaluation for the resonant intersubband conductivity given by Eq. (10). We consider the interaction of electrons with optical phonons at zero temperature and demonstrate that only the broadening of the $1 \to 2$ transition, which is responsible for the absorption, takes place in the passive region while the $2 \to 1$ transition remains narrow (the broadening is determined by the weak elastic scattering).

Within the framework of nonequilibrium diagram technique,[3,13] one describes the transient response on the resonant probe field $E_\perp \exp(-i\omega t)$ based on the linear combination of Green's functions

$$\hat{F}_{t_1 t_2} + \hat{G}^A_{t_1 t_2} - \hat{G}^R_{t_1 t_2} \simeq \int \frac{d\varepsilon}{2\pi\hbar} e^{(i/\hbar)\varepsilon(t_1 - t_2)} \hat{\mathcal{F}}_{\varepsilon(t_1 + t_2/2)} + \widehat{\delta\mathcal{F}}_{t_1 t_2}. \tag{A1}$$

Here $\hat{\mathcal{F}}_{\varepsilon t} = 2f_{\varepsilon t}(\hat{G}^A_\varepsilon - \hat{G}^R_\varepsilon)$ describes the temporal evolution of energy distribution $f_{\varepsilon t}$ governed by the quasiclassic kinetic equation (1), $\hat{G}^{A,R}$ is the advanced (*A*) or retarded (*R*) equilibrium Green's function, and $\widehat{\delta\mathcal{F}}_{t_1 t_2}$ describes the linear response on the perturbation $\widehat{\delta h} \exp$ $\times(-i\omega t)$. Using the ε, t representation we obtain the linearized equation for $\widehat{\delta\mathcal{F}}_\varepsilon \exp(-i\omega t)$ in the following form:

$$\hbar\omega\widehat{\delta\mathcal{F}}_{\varepsilon} - [\hat{h}, \widehat{\delta\mathcal{F}}_{\varepsilon}] - (\widehat{\delta h}\hat{\mathcal{F}}_{\varepsilon-\hbar\omega/2,t} - \hat{\mathcal{F}}_{\varepsilon+\hbar\omega/2,t}\widehat{\delta h})$$

$$= \widehat{\delta\Omega}_{\varepsilon}\hat{G}^{A}_{\varepsilon-\hbar\omega/2} - \hat{G}^{R}_{\varepsilon+\hbar\omega/2}\widehat{\delta\Omega}_{\varepsilon}$$

$$+ \hat{\Sigma}^{R}_{\varepsilon+\hbar\omega/2}\widehat{\delta\mathcal{F}}_{\varepsilon} - \widehat{\delta\mathcal{F}}_{\varepsilon}\hat{\Sigma}^{A}_{\varepsilon+\hbar\omega/2}, \qquad (A2)$$

where $\hat{\Sigma}^{R,A}_{\varepsilon}$ is the R or A self-energies and the integral contribution to this equation is given by

$$\widehat{\delta\Omega}_{\varepsilon} \simeq \sum_{\mathbf{Q}} |C^{(po)}_{Q}|^{2} e^{i\mathbf{Q}\cdot\mathbf{r}} \widehat{\delta\mathcal{F}}_{\varepsilon-\hbar\omega_{o}} e^{-i\mathbf{Q}\cdot\mathbf{r}}. \qquad (A3)$$

Here $C^{(po)}_{Q}$ is the matrix element of the Fröhlich interaction with the bulk phonon mode characterized by the wave vector $\mathbf{Q}=(\mathbf{q}, q_{\perp})$.

For the case of the resonant intersubband excitation, $|\hbar\omega - \varepsilon_{21}| \ll \varepsilon_{21}$, only the component $(\widehat{\delta\mathcal{F}}_{\varepsilon})_{21,\mathbf{p}} \equiv \delta F_{\varepsilon\mathbf{p}}$ appears to be essential. Using the nondiagonal matrix element $\delta h_{21} = (ie/\omega)E_{\perp}v_{\perp}$ we transform Eqs. (A2) and (A3) into

$$(\hbar\omega - \varepsilon_{21} + i\gamma_{p})\delta F_{\varepsilon\mathbf{p}} - \sum_{\mathbf{p}} w_{\mathbf{p}\cdot\mathbf{p}'}\delta F_{\varepsilon-\hbar\omega_{o}\mathbf{p}'}$$

$$= 2\frac{ie}{\omega}E_{\perp}v_{\perp}[f_{\varepsilon-\hbar\omega/2}(G^{A}_{\varepsilon-\hbar\omega/2} - G^{R}_{\varepsilon-\hbar\omega/2})_{11,\mathbf{p}}$$

$$- f_{\varepsilon+\hbar\omega/2}(G^{A}_{\varepsilon+\hbar\omega/2} - G^{R}_{\varepsilon+\hbar\omega/2})_{22,\mathbf{p}}], \qquad (A4)$$

where the broadening energy is given by

$$\gamma_{p} = i[(\hat{\Sigma}^{R}_{\varepsilon+\hbar\omega/2})_{22,\mathbf{p}} - (\hat{\Sigma}^{A}_{\varepsilon+\hbar\omega/2})_{11,\mathbf{p}}]$$

$$\simeq i\sum_{j\mathbf{Q}\mathbf{p}'} |C^{(po)}_{Q}|^{2}\left[\frac{|\langle 2\mathbf{p}|e^{i\mathbf{Q}\cdot\mathbf{r}}|j\mathbf{p}'\rangle|^{2}}{\varepsilon + \hbar\omega/2 - \hbar\omega_{o} + i\lambda}\right.$$

$$\left. - \frac{|\langle 1\mathbf{p}|e^{i\mathbf{Q}\cdot\mathbf{r}}|j\mathbf{p}'\rangle|^{2}}{\varepsilon - \hbar\omega/2 - \hbar\omega_{o} + i\lambda}\right] \qquad (A5)$$

and $w_{\mathbf{p}\cdot\mathbf{p}'}$ is determined by a similar expression which is not essential below. The lower Eq. (A5) is written in the Born approximation and, from the formal point of view, $\lambda \to +0$. If we take into account the elastic scattering, λ should be replaced by the elastic broadening energy.

The Fourier component of current density due to the intersubband transitions under consideration is expressed through $\widehat{\delta F}_{\varepsilon\mathbf{p}}$ according to $\mathbf{j}_{\omega} = -iev_{\perp}\int d\mathbf{p}\int d\varepsilon\widehat{\delta F}_{\varepsilon\mathbf{p}}/(2\pi\hbar)^{2}$. Here we have replaced the perturbation of the density matrix $\widehat{\delta\rho}_{t}$ using the relation $\widehat{\delta\rho}_{t} = (-i\hbar/2)\lim_{t_{1,2}}\widehat{\delta\mathcal{F}}_{t_{1}t_{2}}$. Performing the substitution $\delta F_{\varepsilon\mathbf{p}} = i2eE_{\perp}v_{\perp}\varphi_{\varepsilon\mathbf{p}}/\omega$ we obtain the conductivity

$$\sigma_{\omega} = \frac{e^{2}|v_{\perp}|^{2}}{\pi}\int\frac{d\mathbf{p}}{(2\pi\hbar)^{2}}\int d\varepsilon\varphi_{\varepsilon\mathbf{p}}. \qquad (A6)$$

The function $\varphi_{\varepsilon\mathbf{p}}$ is governed by the integral equation

$$(\hbar\omega - \varepsilon_{21} + i\gamma_{p})\varphi_{\varepsilon\mathbf{p}} - \sum_{\mathbf{p}} w_{\mathbf{p}\cdot\mathbf{p}'}\varphi_{\varepsilon-\hbar\omega_{o}\mathbf{p}}$$

$$= f_{\varepsilon-\hbar\omega/2}(G^{A}_{\varepsilon-\hbar\omega/2} - G^{R}_{\varepsilon-\hbar\omega/2})_{11,\mathbf{p}}$$

$$- f_{\varepsilon+\hbar\omega/2}(G^{A}_{\varepsilon+\hbar\omega/2} - G^{R}_{\varepsilon+\hbar\omega/2})_{22,\mathbf{p}}, \qquad (A7)$$

which is obtained from Eq. (A4).

Next we write the resonant conductivity (A6) for the case of the δ-like electron distribution $f_{\varepsilon} = (n_{ex}/2\rho_{2D})\delta(\varepsilon_{ex} - \varepsilon)$ with the excitation energy ε_{ex} localized in the interval $(\hbar\omega_{o} - \varepsilon_{ex}, \hbar\omega_{o})$. Due to the weakness of the integral term in Eq. (A7) we obtain the conductivity in the form

$$\sigma_{\omega} = \frac{e^{2}|v_{\perp}|^{2}}{2\pi}n_{ex}\int d\varepsilon_{p}\left[\frac{(G^{A}_{\varepsilon-\hbar\omega/2} - G^{R}_{\varepsilon-\hbar\omega/2})_{11,\mathbf{p}}}{\hbar\omega - \varepsilon_{21} + i\gamma_{p|\varepsilon\to\varepsilon_{ex}+\hbar\omega/2}}\right.$$

$$\left. - \frac{(G^{A}_{\varepsilon-\hbar\omega/2} - G^{R}_{\varepsilon-\hbar\omega/2})_{22,\mathbf{p}}}{\hbar\omega - \varepsilon_{21} + i\gamma_{p|\varepsilon\to\varepsilon_{ex}-\hbar\omega/2}}\right]. \qquad (A8)$$

The spectral densities in the numerators

$$(G^{A}_{\varepsilon-\hbar\omega/2} - G^{R}_{\varepsilon-\hbar\omega/2})_{jj,\mathbf{p}} \simeq \frac{i2\lambda}{(\varepsilon_{ex} - \varepsilon_{jp})^{2} + \lambda^{2}}, \qquad (A9)$$

are written through the δ-functions if $\lambda \to +0$. As a result, Eq. (A8) is transformed into Eq. (10) with the elastic broadening energy in the second contribution while the optical phonon induced broadening appears in the first term. The corresponding broadening energy is determined as $\Gamma = \mathrm{Re}\,\gamma_{p}|_{\varepsilon_{p}\to\varepsilon_{ex},\varepsilon\to\varepsilon_{ex}+\hbar\omega/2}$ or

$$\Gamma \simeq \frac{2\pi^{2}e^{2}\hbar\omega_{o}}{\epsilon^{*}V}\sum_{q_{\perp}\mathbf{p}'}\frac{|\langle 2|e^{iq_{\perp}z}|1\rangle|^{2}}{|\mathbf{p} - \mathbf{p}'|/\hbar^{2} + q_{\perp}^{2}}$$

$$\times \delta(\varepsilon_{ex} + \varepsilon_{21} - \hbar\omega_{o} - \varepsilon_{1p'})|_{\varepsilon_{p}\to\varepsilon_{ex}}, \qquad (A10)$$

where V is the normalization volume and the effective dielectric permittivity, $\epsilon^{*} = (\epsilon_{o} - \epsilon_{\infty})/\epsilon_{o}\epsilon_{\infty}$, is introduced through the static and high-frequency dielectric permittivities, ϵ_{o} and ϵ_{∞}. Performing the integration over the energy one obtains

$$\Gamma \simeq \frac{e^{2}\hbar\omega_{o}}{4\epsilon^{*}}\rho_{2D}\int dq_{\perp}\int_{0}^{2\pi}d\varphi\frac{|\langle 2|e^{iq_{\perp}z}|1\rangle|^{2}}{q_{\perp}^{2} + Q_{\varphi}^{2}}, \qquad (A11)$$

where the denominator contains the factor $Q_{\varphi}^{2} = (p_{ex}^{2} + \tilde{p}_{ex}^{2} - 2p_{ex}\tilde{p}_{ex}\cos\varphi)/\hbar^{2}$ with the characteristic momenta $p_{ex} = \sqrt{2m\varepsilon_{ex}}$ and $\tilde{p}_{ex} = \sqrt{2m[\varepsilon_{ex} - (\hbar\omega_{o} - \varepsilon_{21})]}$.

---

*Electronic address: ftvasko@yahoo.com

†Electronic address: ajhernan@ull.es

[1] J. Shah, *Ultrafast Spectroscopy of Semiconductors and Semiconductor Nanostructures* (Springer, Berlin, 1999); F. Rossi and T. Kuhn, Rev. Mod. Phys. **74**, 895 (2002).

[2] E. Gornick and R. Kerstling, Semicond. Semimetals **67**, 389 (2001); V. N. Bondar, A. T. Dalakyan, L. E. Vorobev, D. A. Firsov, and V. N. Tulupenko, JETP Lett. **70**, 265 (1999); M. A. Odnoblyudov, I. N. Yassievich, M. S. Kagan, and K. A. Chao, Phys. Rev. B **62**, 15291 (2000).

[3] H. Haug and A.-P. Jauho, *Quantum Kintetics in Transport and Optics of Semiconductors* (Springer, Berlin, 1996).

[4] F. T. Vasko and A. Kuznetsov, *Electronic States and Optical Transitions in Semiconductor Heterostructures* (Springer, New York, 1998).

[5] F. Prengel and E. Scholl, Phys. Rev. B **59**, 5806 (1999); J. Schilp, T. Kuhn, and G. Mahler, *ibid.* **50**, 5435 (1994).

[6] S. E. Esipov and Y. B. Levinson, Adv. Phys. **36**, 331 (1987).

[7] F. T. Vasko, JETP Lett. **79**, 431 (2004).

[8] A. Hernandez-Cabrera, P. Aceituno, and F. T. Vasko, Phys. Rev. B **67**, 045304 (2003); S. Khanngern and I. A. Larkin, *ibid.* **64**, 115313 (2001).

[9] B. S. Williams, S. Kumar, H. Callebaut, Q. Hu, and J. L. Reno, Appl. Phys. Lett. **83**, 5142 (2003); H. N. Rutt, Z. J. Xin, and I. A. Tan, J. Phys. D **35**, 1907 (2002); T. G. Ulmer, M. Hanna, B. R. Washburn, S. E. Ralph, and A. J. Spring-Thorpe, IEEE J. Quantum Electron. **38**, 19 (2002); M. Rochat, L. Ajili, H. Willenberg, J. Faist, H. Beere, G. Davies, E. Linfield, and D. Ritchie, Appl. Phys. Lett. **81**, 1381 (2002).

[10] P. Kinsler, P. Harrison, and R. W. Kelsall, Phys. Rev. B **58**, 4771 (1998); M. Hartig, J. D. Ganiere, P. E. Selbmann, B. Deveaud, and L. Rota, *ibid.* **60**, 1500 (1999); K. Kempa, P. Bakshi, J. Engelbrecht, and Y. Zhou, *ibid.* **61**, 11083 (2000).

[11] I.-K. Oh, J. Singh, A. Thilagam, and A. S. Vengurlekar, Phys. Rev. B **62**, 2045 (2000); R. Kumar, A. S. Vengurlekar, S. S. Prabhu, J. Shah, and L. N. Pfeiffer, *ibid.* **54**, 4891 (1996).

[12] M. A. Stroscio and M. Dutta, *Phonons in Nanostructures* (Cambridge University Press, Oxford, 2001); P. Kinsler, R. M. Kelsall, and P. Harrison, Physica B **263**, 507 (1999).

[13] E. M. Lifshitz and L. P. Pitaevskii, *Physical Kinetics* (Elsevier, Amsterdam, 1981).